Protein Cell 2013, 4(2): 142–154
DOI 10.1007/s13238-012-2088-4

Protein & Cell

RESEARCH ARTICLE

Structural and biochemical studies of RIG-I antiviral signaling

Miao Feng[1*], Zhanyu Ding[2*], Liang Xu[1*], Liangliang Kong[2], Wenjia Wang[1], Shi Jiao[1], Zhubing Shi[1], Mark I. Greene[3], Yao Cong[2]✉, Zhaocai Zhou[1]✉

[1] State Key Laboratory of Cell Biology, Institute of Biochemistry and Cell Biology, Shanghai Institutes for Biological Sciences, Chinese Academy of Sciences, Shanghai 200031, China
[2] State Key Laboratory of Molecular Biology, Institute of Biochemistry and Cell Biology, Shanghai Institutes for Biological Sciences, Chinese Academy of Sciences, Shanghai 200031, China
[3] Department of Pathology and Laboratory Medicine, University of Pennsylvania, PA 19104, USA
✉ Correspondence: cong@sibcb.ac.cn (Y. Cong), zczhou@sibcb.ac.cn (Z. Zhou)
Received August 23, 2012 Accepted November 29, 2012

ABSTRACT

Retinoic acid-inducible gene I (RIG-I) is an important pattern recognition receptor that detects viral RNA and triggers the production of type-I interferons through the downstream adaptor MAVS (also called IPS-1, CARDIF, or VISA). A series of structural studies have elaborated some of the mechanisms of dsRNA recognition and activation of RIG-I. Recent studies have proposed that K63-linked ubiquitination of, or unanchored K63-linked polyubiquitin binding to RIG-I positively regulates MAVS-mediated antiviral signaling. Conversely phosphorylation of RIG-I appears to play an inhibitory role in controlling RIG-I antiviral signal transduction. Here we performed a combined structural and biochemical study to further define the regulatory features of RIG-I signaling. ATP and dsRNA binding triggered dimerization of RIG-I with conformational rearrangements of the tandem CARD domains. Full length RIG-I appeared to form a complex with dsRNA in a 2:2 molar ratio. Compared with the previously reported crystal structures of RIG-I in inactive state, our electron microscopic structure of full length RIG-I in complex with blunt-ended dsRNA, for the first time, revealed an exposed active conformation of the CARD domains. Moreover, we found that purified recombinant RIG-I proteins could bind to the CARD domain of MAVS independently of dsRNA, while S8E and T170E phosphorylation-mimicking mutants of RIG-I were defective in binding E3 ligase TRIM25, unanchored K63-linked polyubiquitin, and MAVS regardless of dsRNA. These findings suggested that phosphorylation of RIG inhibited downstream signaling by impairing RIG-I binding with polyubiquitin and its interaction with MAVS.

KEYWORDS RIG-I, MAVS, antiviral signaling, polyubiquitin, phosphorylation

INTRODUCTION

The innate immune system can detect invasion of microbial pathogens through germline-encoded pattern recognition receptors (PRRs) (Kumar et al., 2009; Takeuchi and Akira, 2010). The PRRs recognize pathogen-associated molecular patterns (PAMPs) that are structurally conserved among microbes. This process then triggers immune signaling of host cells, leading to upregulation of proinflammatory cytokines and expression of classes of antimicrobial peptides (Janeway and Medzhitov, 2002). Four subfamilies of PRRs have been identified to date, including membrane-bound Toll-like receptors (TLRs), C-type lectin receptors (CLRs), and cytoplasmic proteins such as NOD-like receptors (NLRs) and retinoic acid-inducible gene-I-like receptors (RLRs) (Takeuchi and Akira, 2010).

RLRs include three members, RIG-I (retinoic-acid-inducible gene-I; also called DDX58), MDA5 (melanoma differentiation-associated gene 5) and LGP2 (laboratory of genetics and physiology 2) (Yoneyama et al., 2004). These protein species are involved in detecting viral RNAs and initiating signal transduction cascades that leads to the expression of type I interferons.

RIG-I is evolutionarily conserved RNA helicase in verte-

*These authors contributed equally to the work.

brates and contains two N-terminal tandem caspase activation and recruitment domains (CARDs), a DExD-box RNA helicase/ATPase domain and a C-terminal regulatory domain (CTD), also termed repressor domain (RD) (Fig. 1A) (Yoneyama et al., 2005; Saito et al., 2007; Lu et al., 2010). RIG-I recognizes and unwinds viral dsRNA employing the CTD and

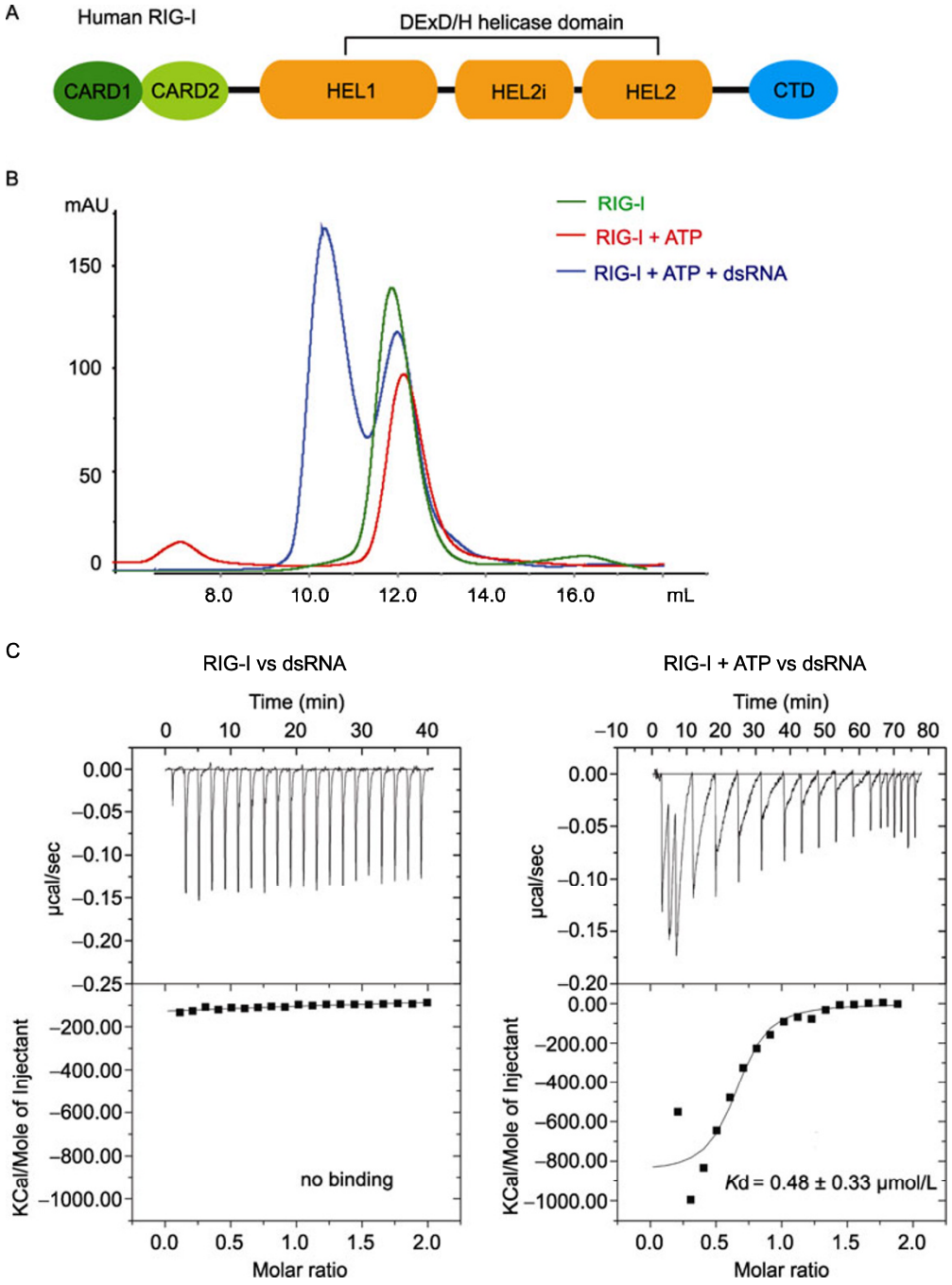

Figure 1. dsRNA and ATP induces dimerization of full length RIG-I. (A) Schematic illustration of domain organization of human RIG-I. RIG-I comprises two N-terminal tandem CARD domains (colored in green), a DExD-box RNA helicases (colored in orange), which consists of a helicase insertion domain (HEL2i) and helicase domain 1 (HEL1) and 2 (HEL2), and a C-terminal domain (CTD) (colored in cyan). (B) Gel filtration chromatography of full length RIG-I with or without dsRNA. Proteins of full length RIG-I alone (green) or preincubted with ATP (red) or synthesized 14-bp blunt-ended dsRNA (blue) were subject to gel filtration analysis. (C) RNA binding of full length RIG-I studied by isothermal titration calorimetry (ITC). Left panel: ITC of 14-bp blunt-ended dsRNA with a solution of full length RIG-I in the absence of ATP. Right panel: ITC of 14-bp blunt-ended dsRNA with a solution of full length RIG-I in the presence of ATP. In each figure, the upper panel shows the experimental data for the titration, whereas the lower panel shows the integrated binding isotherm for each injection and fitted to a single-site binding curve.

helicase domain in the presence of ATP. In addition to dsRNA, RIG-I also detects single-stranded RNA bearing 5′-phosphates to trigger antiviral responses (Pichlmair et al., 2006). RNA binding induces a conformational change of RIG-I to form dimers (Yoneyama et al., 2004). Subsequently, the N-terminal CARD domains of RIG-I mediate downstream signaling by interacting with the adaptor protein MAVS (also known as VISA, IPS-1, and CARDIF), located on mitochondrial outer membranes (Kawai et al., 2005; Meylan et al., 2005; Xu et al., 2005).

Structural studies of RIG-I individual domains have provided some atomic insight into the mechanism of recognition of virus dsRNA and activation of RIG-I (Leung and Amarasinghe, 2012). RIG-I is thought to assume an autoinhibitory conformation in which the CTD is flexibly attached to the helicase and the CARDs are clamped between the two moieties of the helicase domain. As such, the function of the tandem CARD domains is repressed and RIG-I has a low affinity for ATP and dsRNA binding (Kowalinski et al., 2011). Upon virus infection, dsRNA binds to the cleft of the CTD which ultimately induces conformational changes of RIG-I to relieve structural constraints and functional repression of the CARD domains. Activated RIG-I molecules are recruited to mitochondria where the released CARD domains bind to MAVS (Kawai et al., 2005; Meylan et al., 2005; Xu et al., 2005; Liu et al., 2012). MAVS then activates the cytosolic protein kinases IKK and TBK1, which in turn activate the transcriptional factors NF-κB and IRF3, respectively. NF-κB, IRF3 and other transcriptional factors function together in the nucleus to induce the expression of type-I interferons and other antiviral molecules. During this process, MAVS can form functional prion-like aggregates on mitochondrial membrane to propagate the antiviral signaling (Hou et al., 2011).

Recent studies indicated that the regulation of RIG-I signaling involves post-translational modifications such as ubiquitination and phosphorylation. After binding to viral dsRNA, the CARD domains of RIG-I undergo ubiquitination through the E3 ubiquitin ligase TRIM25 (tripartite motif-containing protein 25) (Gack et al., 2007). TRIM25 interacts with the first CARD domain of RIG through its SPRY domain, and exclusively conjugates K63-linked polyubiquitin (polyUb) on RIG-I and consequently facilitates downstream signal transduction through interacting with MAVS (Gack et al., 2008). Meanwhile, unanchored K63-linked polyUb may be necessary and sufficient to activate the RIG-I pathway and induce the expression of type-I interferons (Zeng et al., 2010). PolyUb chains appear to induce high-order oligomerization of RIG-I, which may play a pivotal role in augmenting the antiviral signaling cascades through MAVS (Jiang et al., 2012).

Phosphorylation has been identified as an important negative regulatory mechanism of RIG-I signaling pathway (Gack et al., 2010). It was found that S8 and T170 in the tandem CARD domains of RIG-I are constitutively phosphorylated under physiological conditions (Gack et al., 2010; Nistal-Villan et al., 2010). The S8E and T170E mutants of RIG-I appear to inhibit TRIM25 binding. Protein kinase C (PKC) has been identified as the primary kinase responsible for the phosphorylation of RIG-I and therefore repression of RIG-I-mediated MAVS signaling pathway (Maharaj et al., 2012).

Structural and biochemical analyses of RIG-I antiviral signaling pathway using various purified recombinant proteins was undertaken. We confirmed that the dimerization of full length RIG-I occurs upon dsRNA binding. These studies revealed features of the conformational rearrangements of the CARD domains that occur upon activation. RIG-I can bind to the CARD domain of MAVS, but phosphorylation at sites S8 or T170 of RIG-I prevents the CARD domains from binding to MAVS.

RESULTS

dsRNA and ATP induce dimerization of full length RIG-I to form a 2:2 complex

As aforementioned, RIG-I mainly consists of three functional domains as illustrated in Fig. 1A. Previous studies concerning the crystal structures of RIG-I C-terminal domain (CTD) bound to 5′ppp and blunt-ended dsRNA provide some mechanistic models regarding recognition of viral RNA (Lu et al., 2010, 2011). Notably, these studies suggested a complex of 2:1 stoichiometry between CTD of RIG-I and dsRNA, where each terminus of the dsRNA binds one CTD.

To better understand the dsRNA binding properties of RIG-I in full length context, we expressed RIG-I in *Escherichia coli* and purified the recombinant proteins for *in vitro* experiments. A synthesized 14-bp GC-rich dsRNA was used for RIG-I binding analysis. RIG-I protein alone was subject to Superdex-200 gel filtration chromatography. According to our standard curve, the molecular weight of RIG-I alone was 110 kDa, indicating its monomeric state. Neither ATP alone (Fig. 1B) nor dsRNA alone (Fig. 1C) could change the oligomeric status of full length RIG-I. Only in the presence of ATP, dsRNA could bind to full length RIG-I with high affinity (*K*d of 0.48 ± 0.33 μmol/L) (Fig. 1C). Moreover, our gel filtration assays showed that in the presence of both ATP and the 14-bp blunt-ended dsRNA, RIG-I was eluted at ~200 kDa, corresponding to the molecular weight of RIG-I dimer. These observations suggested that dsRNA could induce full length RIG-I to form dimer in the presence of ATP.

By examining the gel filtration curve of RIG-I mixed with dsRNA in 2:1 molar ratio, we found that part of RIG-I proteins remained in the monomeric fraction (Fig. 2A, left panel). However, the mixture of RIG-I and dsRNA in equal molar ratio were mainly eluted in a fraction corresponding to molecular weight of ~200 kDa (Fig. 2A, right panel). We therefore speculated that dsRNA binding triggered conformational changes of RIG-I monomers to form a homodimer with each RIG-I molecule recognizing and accommodating one dsRNA. To further verify the stoichiometry of RIG-I:dsRNA complex, we performed dynamic light scattering (DLS) to detect the molecular weight and homogenicity of full length RIG-I mixed with dsRNA in different molar ratio. While RIG-I alone was a

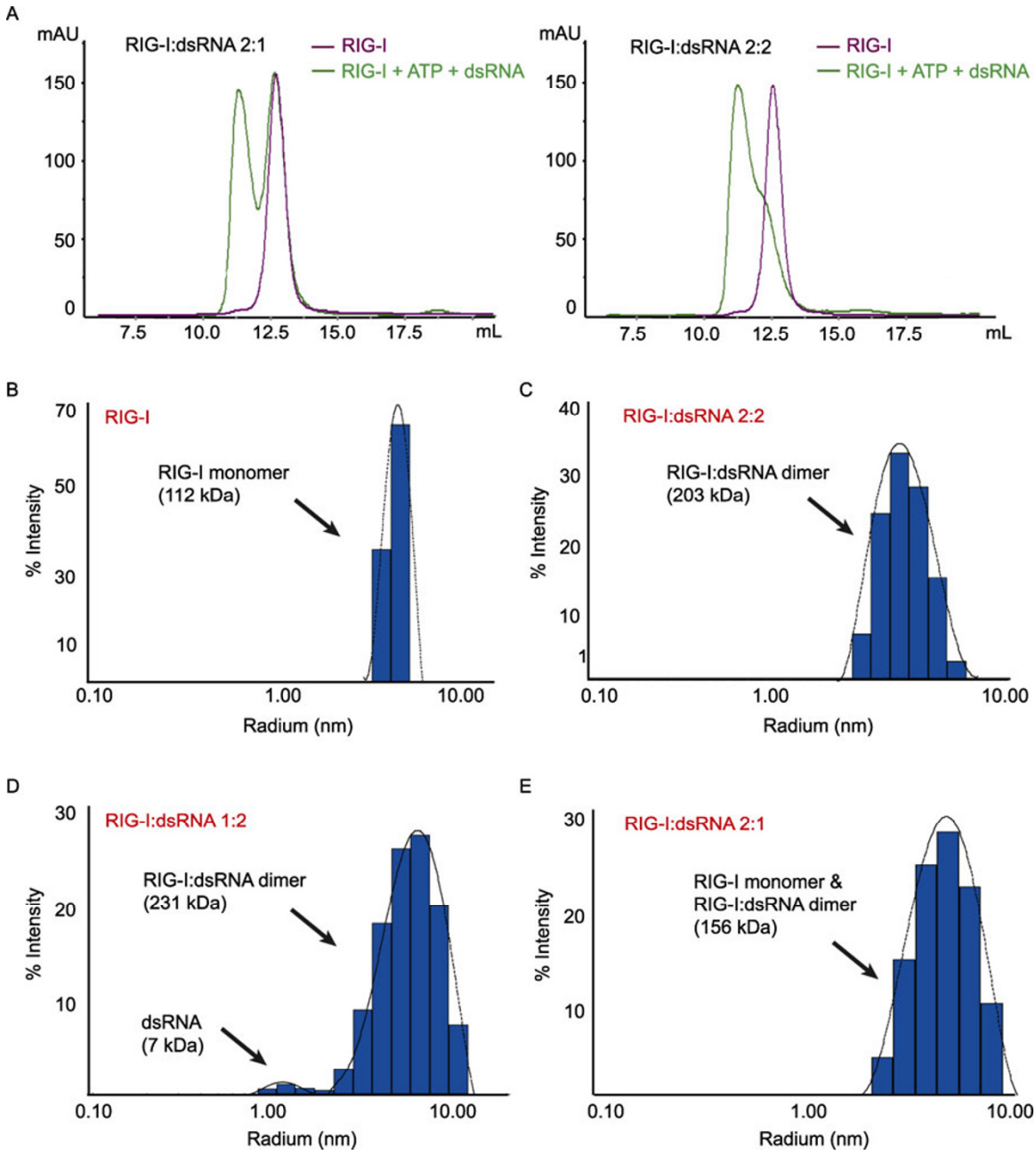

Figure 2. Full length RIG-I and dsRNA formed a 2:2 complex. (A) Gel filtration chromatography of full length RIG-I with dsRNA. Left panel: RIG-I with dsRNA in a 2:1 molar ratio; Right panel: RIG-I with dsRNA in a 2:2 molar ratio. (B–E) Dynamic light scattering (DLS) assays of RIG-I with dsRNA in different molar ratios. (B) In the absence of dsRNA, RIG-I was a monomer and the corresponding molecular weight was 112 kDa. (C–E) Full length RIG-I mixed with dsRNA in molar ratio 1:1, 1:2 or 2:1. The corresponding molecular weights were 203 kDa, 231 kDa and 156 kDa, respectively. All mixed samples of RIG-I and dsRNA contained 1 mmol/L ATP.

monomer (Fig. 2B), the sample of RIG-I mixture with dsRNA in equal molar ratio was most homogeneous with a molecular weight of around 203 kDa (Fig. 2C), indicating that dsRNA induced RIG-I to form a homodimer. This result was consistent with the estimates from gel filtration analysis. Moreover, excessive amount of either RIG-I or dsRNA significantly reduced the homogenicity of mixtures, leading to multiple molecular species in solution (Fig. 2D and 2E). Taken together, our results indicated that full length RIG-I appeared to bind dsRNA with a molecular ratio of 2:2 instead of 2:1 that was previously reported for the complex of RIG-I CTD and dsRNA (Lu et al., 2011).

Electron microscopic structure of RIG-I in complex with blunt-ended dsRNA

The crystal structures of the helicase and CTD domains of human RIG-I bound to dsRNA, as well as the CARDs and helicase domains of duck RIG-I have been determined (Jiang et al., 2011; Kowalinski et al., 2011). However, the structural information of full length RIG-I remains unavailable. We then utilized negative staining electron microscope (EM) to characterize the structural features of full length RIG-I in complex with blunt-ended dsRNA (Fig. 3A). The complex was assembled *in vitro* by mixing purified human full length RIG-I proteins with the synthesized 14-bp blunt-ended dsRNA, followed by gel filtration. Target fractions corresponding to dimers of RIG-I in complex with dsRNA were pooled and concentrated for EM study.

3D density map of the full length RIG-I-dsRNA complex (Fig. 3B) was constructed by single particle analysis of 10,991 particles utilizing EMAN1 package (Ludtke et al., 1999, 2001). We first calculated a density map without imposing any symmetry, which revealed the existence of a 2-fold symmetry in the map (Fig. S1). Thus the 2-fold symmetry was imposed in the subsequent reconstruction process. Comparison of the 3D density map and the reference-free 2D class averages revealed a reasonable correspondence between them (Fig. S2A), indicating the reliability of our 3D density map. Resolution of the final map was assessed to be approximately 15.0 Å based on a criterion of 0.5 Fourier Shell Correlation (FSC) (Fig. S2B). Moreover, the measured volume of our density map corresponded to a molecular mass of approximately 200 kDa, which was similar to that of RIG-I dimer.

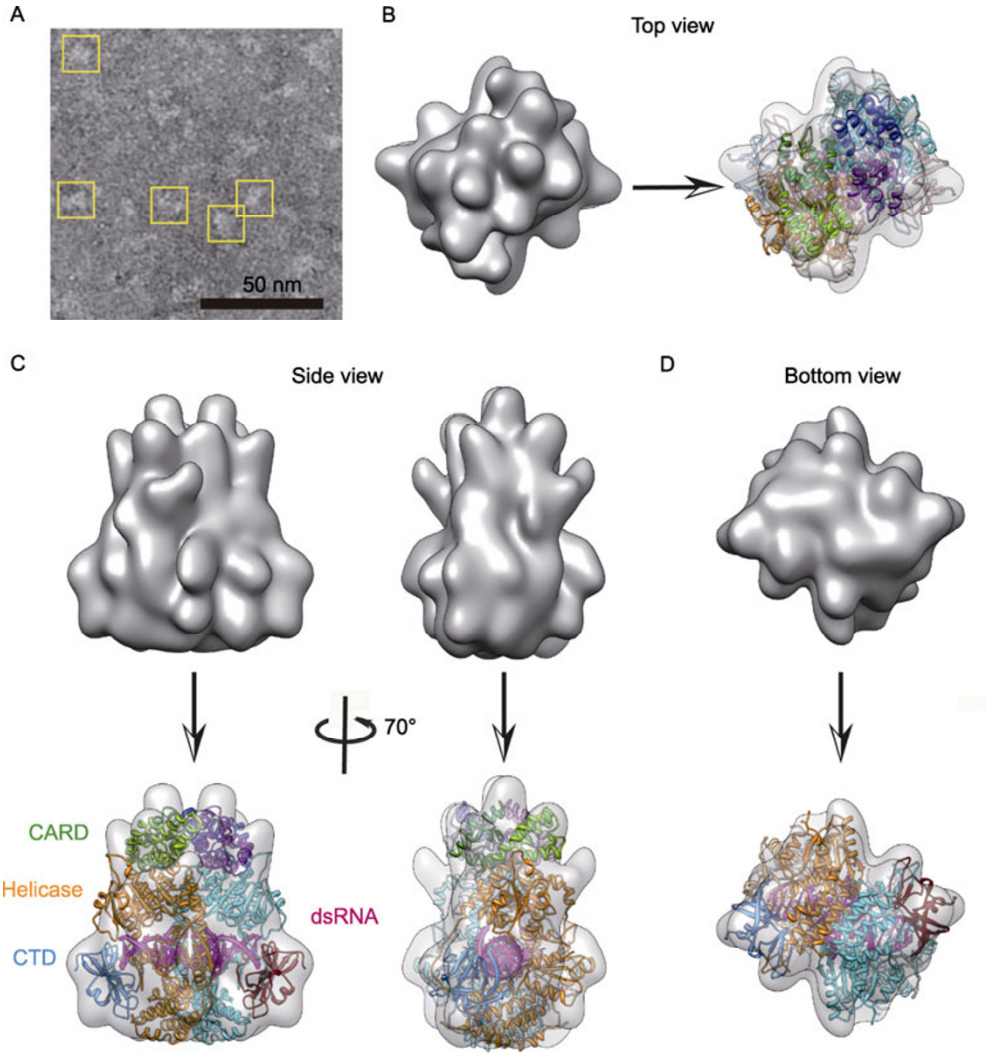

Figure 3. EM structure of full length RIG-I in complex with dsRNA. (A) A typical negative stain CCD image of RIG-I in complex with dsRNA. Representative particles are highlighted by yellow boxes. (B–D) Different views of the final EM density map filtered to 15 Å and corresponding views of models fitted into the density map with different domains. For the left copy of RIG-I, the CARDs, helicase and CTD domains were colored in green, orange and cyan respectively. For the purpose of clarity, the right copy of RIG-I was colored otherwise. The dsRNA was colored in magenta.

To further interpret the density map in more structural details, we fitted the homologous crystal models into the map (Fig. 3B–D). The crystal structure of the helicase domain (PDB ID: 3TMI) (Jiang et al., 2011) and a comparative model of the CARD domains were fitted independently into our density map by rigid-body fitting using Situs package (Wriggers et al., 1999). The cross-correlation score between the map and model was 0.88 calculated by using EMAN program *foldhunter P*. Moreover, a difference map was calculated between our density map and a blurred map at 15 Å generated from our pseudo atomic model (Fig. S3), indicating a reasonable fitting of our model.

Our fitting clearly demonstrated that the density map contains two RIG-I monomers side by side bound with two individual dsRNA, forming a 2:2 RIG-I:dRNA complex. This observation revealed without ambiguity that RIG-I forms a homodimer in the presence of dsRNA, consistent with our gel filtration and DLS results. Moreover, the helicase and CTD domains were automatically fitted into the lower portion of the density map (Fig. 3B–D). The fitting suggested that, for the RIG-I monomer within the dimer, the CTD domains were exposed outside while the helicase domain remained inside the molecule. The CARD domains were located in the upper part of the EM density map, indicating the approximate location of the relived CARD domains upon the dimerization of RIG-I when triggered by dsRNA binding (Fig. 3C). The relative orientation of the CARD domains to the helicase and CTD domains, to our knowledge, revealed for the first time an active conformation of RIG-I in full length. Of particular note, the two tandem CARD domains had to be treated separately as individual rigid bodies to obtain the best fit into our EM density map, indicating conformational rearrangements of the CARD domains during RIG-I dimerization. This observation differed from a previous report suggesting that the tandem CARD domains of RIG-I formed a rigid functional unit (Kowalinski et al., 2011). Taken together, these results revealed an active conformation of RIG-I:dsRNA complex, in which the two RIG-I monomers pack against each other mainly through their helicase domains in a back to back mode with CTD domains protruding outside in opposite directions. As such the CARD domains of the two RIG-I molecules were brought together and structurally more exposed.

dsRNA promotes specific binding of K63-linked polyUb to RIG-I

Previous study suggested that unanchored K63-linked polyUb are required for full activation of RIG-I-mediated MAVS signaling (Zeng et al., 2010). Although it has been proposed that only K63-linked polyUb can activate RIG-I and eventually cause dimerization of IRF3, the binding of different types of polyUb chains to RIG-I has not been examined in detail. Using purified recombinant proteins of RIG-I and polyUb chains, we tested interactions between full length RIG-I and K11- or K48- or K63-linked Ub3 in the presence or absence of dsRNA and ATP.

Our pull-down assay indicated that K11-linked Ub3 was incapable of binding to RIG-I with or without dsRNA (Fig. 4A, lanes 1 and 4). K48-linked Ub3 weakly interacted with RIG-I in the presence of dsRNA and ATP (Fig. 4A, lane 5). However, K63-linked Ub3 bound to full length RIG-I no matter preincubating with dsRNA or not (Fig. 4A, lanes 3 and 6). But the binding of K63-linked Ub3 was enhanced in the presence of dsRNA and ATP. The result of western blot was in accordance with that of the SDS-PAGE (Fig. S4). This enhanced polyUb binding could be explained by our EM analysis showing conformational rearrangements of the CARD domains of RIG-I upon dsRNA binding. The conformational rearrangements trigged by dsRNA ligation could relive the CARD domains of RIG-I from the repression of the helicase domain, rendering them more flexible and fully accessible to unanchored polyUb chains (Luo et al., 2012) (Fig. 4E). Taken together, these results suggested that RIG-I selectively bound to K63-linked polyUb, supporting the notion that full activation of RIG-I signaling required K63-linked polyUb binding in a dsRNA dependent manner.

Ubiquitination-defective and phosphorylation-mimicking mutations of RIG-I impair K63-linked polyUb binding

Both ubiquitination of K172 or binding of unanchored K63-linked polyUb have been implicated in promoting RIG-I-mediated antiviral signaling (Gack et al., 2007; Zeng et al., 2010). It has been found that mutations of T55I and K172R of RIG-I may abolish TRIM25-mediated ubiquitination of the CARD domains. A recent study identified that PKC induced phosphorylation of RIG-I functionally antagonizes the ubiquitination-mediated activation of RIG-I signaling (Gack et al., 2010). Phoshporylation-mimicking at sites S8 and T170 of RIG-I suppresses ubiquitination of the CARD domains and therefore inhibits RIG-I antiviral activity. However, it has not been clearly defined whether phosphorylation at sites S8 and T170, as well as ubiquitination defective mutations of RIG-I regulates the binding of unanchored polyUb chains. To address these questions, we performed pull-down assay using purified wild-type and mutant (S8E, T55I, T170E and K172R) RIG-I proteins in full length.

Wild-type and mutant RIG-I proteins were incubated with the synthesized 14-bp blunt-ended dsRNA and ATP for 30 min in a buffer containing 20 mmol/L HEPES (pH7.5) and 100 mmol/L NaCl, and then used pull-down assay to detect binding of purified K63-linked Ub3. To avoid non-specific binding, the pull-down samples were washed with the same buffer containing 50 mmol/L imidazole. As shown in Fig. 4B, wild-type RIG-I could efficiently bind to K63-linked Ub3 in the presence of dsRNA (lane 2). However, RIG-I mutants S8E and T55I exhibited decreased binding of K63-linked Ub3 (lanes 3 and 4). Furthermore, RIG-I mutants T170E and K172R did not show detectable binding of K63-Ub3 (Fig. 4B). These results indicated that phosphorylation-mimicking at

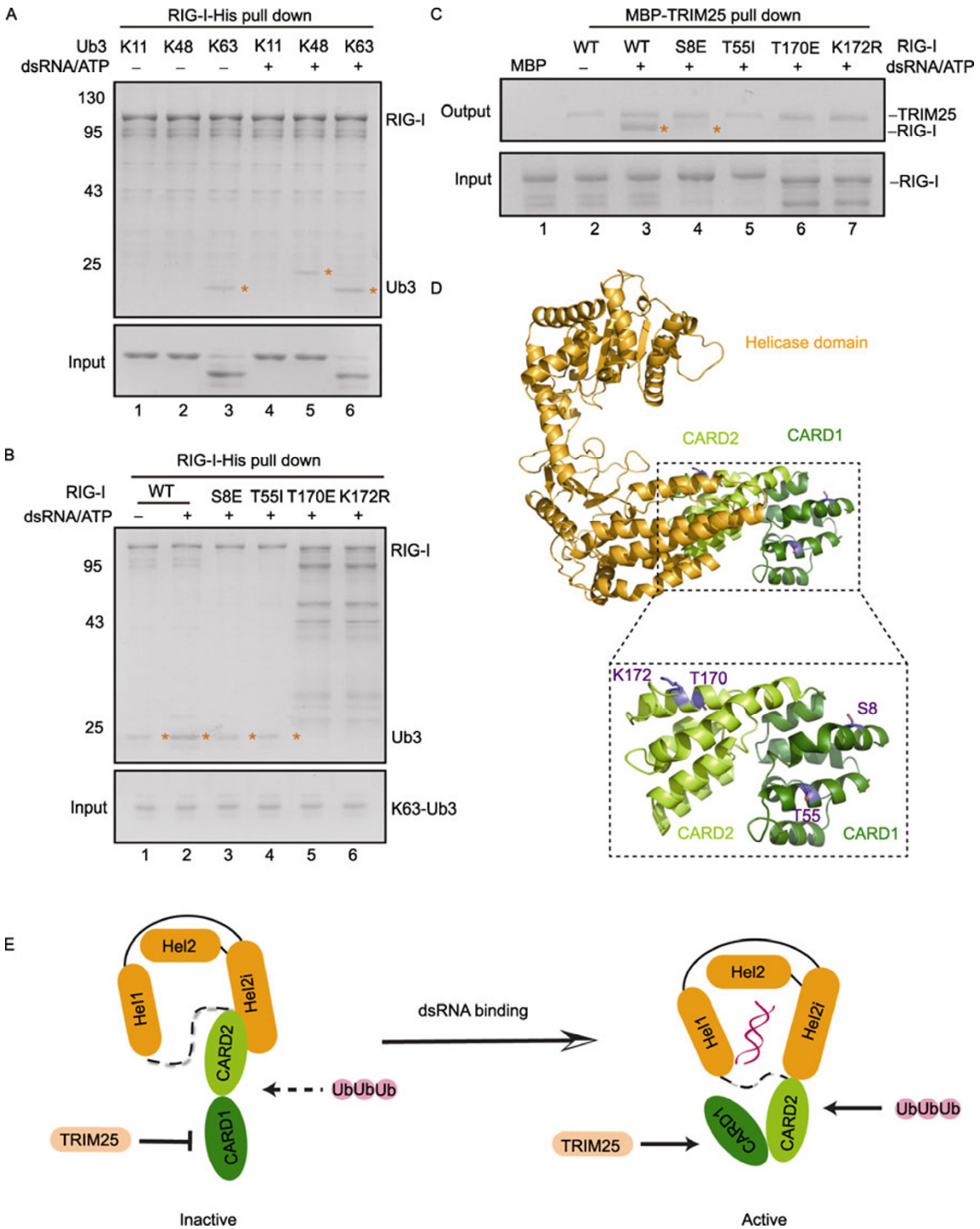

Figure 4. *In vitro* binding of K63-Ub3 and TRIM25 to full length RIG-I. (A) His pull-down of wild-type (WT) full length RIG-I with K11- or K48- or K63-linked Ub3. Purified RIG-I-cHis proteins with and without dsRNA were coupled on Ni^{2+}-NTA beads and incubated with K11- or K48- or K63-linked Ub3, respectively. Samples were analyzed by SDS-PAGE. The asterisks denote various forms of Ub3 bound with RIG-I. (B) Binding of K63-Ub3 to various mutants of full length RIG-I. The experimental set is similar to (A). Clearly, mutations of S8E and T55I decreased K63-Ub3 binding to RIG-I (lanes 3, 4 and 5), while mutations of T170E and K172R greatly impaired K63-Ub3 binding to RIG-I (lanes 6 and 7). The asterisks denote K63-Ub3 bound to RIG-I. (C) Mutations of S8E, T55I, T170E and K172R disrupted TRIM25 binding to RIG-I. MBP was used as control (lane 1). The asterisks indicate RIG-I pulled down by MBP-TRIM25. (D) Structure of the CARDs and helicase domains of human RIG-I. The structure was modeled from crystal structure of duck RIG-I (PDB ID: 4A2W) by the SWISS-MODEL Repository. The CARD1, CARD2 and helicase domains are colored in green, light green and orange, respectively. The mutations of S8E, T55I, T170E and K172R are shown in slate. (E) A model of the conformational rearrangement of RIG-I CARD domains.

sites S8 and T170 of RIG-I impaired binding of unanchored K63-linked polyUb *in vitro*.

Phosphorylation-mimicking of RIG-I disrupts its direct interaction with TRIM25

Previous cell based study indicated that the E3 ubiquitin ligase TRIM25 mediates RIG-I antiviral activity by introducing K63-linked ubiquitination at site K172 of RIG-I (Gack et al., 2007, 2008). To detect a direct interaction between full length RIG-I and TRIM25, we performed pull-down assay using purified recombinant proteins of RIG-I and TRIM25. As shown in Fig. 4C, TRIM25 binding to wild-type RIG-I was dependent on dsRNA and ATP (lanes 2 and 3), consistent with the notion that dsRNA-induced conformational rearrangements of the repressed tandem CARD domains is a prerequisite for TRIM25 binding.

Next we assessed the effect of various mutations on the direct interaction between RIG-I and TRIM25. As expected, mutations T55I and K172R of RIG-I abrogated TRIM25 binding (Fig. 4C, lanes 5 and 7). The RIG-I mutant S8E showed a markedly reduced binding of TRIM25 (lane 4), while the mutant T170E was completely disabled for TRIM25 binding (lane 6), suggesting that phosphorylation-mimicking of CARD domains directly inhibited TRIM25 binding. It is likely that the phosphorylation of RIG-I may directly alter the surface charge required for TRIM25 binding, or introduce steric hindrance to prevent binding.

Interestingly, when compared with mutations of S8E and T55I, which are located in the first CARD domain of RIG-I, mutations of T170E and K172R, which are located within the second CARD domain caused more severe effects on the binding of both TRIM25 and unanchored K63-linked Ub3, highlighting a primary role of the second CARD domain in polyUb-related activation of RIG-I. This notion is also supported by the structural organization of the tandem CARD domains in the inactive state of RIG-I. The first CARD is more exposed while the second one is strictly constrained by the helicase domain (Fig. 4D).

Phosphorylation-mimicking of RIG-I inhibits its interaction with MAVS

Upon activation, the tandem CARD domains of RIG-I interact with the CARD domain of MAVS to transduce antiviral signaling. To detect direct interactions between RIG-I and MAVS, we performed pull-down assay using purified recombinant proteins of full length His-tagged RIG-I and MBP-tagged CARD domain of MAVS. As shown by the two-direction pull-down in Fig. 5A and 5B, RIG-I could bind to the CARD domain of MAVS independent of dsRNA and ATP. This observation could be explained by the crystal structure of the ligand-free RIG-I-ΔCTD which revealed a head-to-tail conformation of the tandem CARD domains (Kowalinski et al., 2011). Thus even in its inactive state, the first CARD domain of RIG-I is exposed and does not contact with the helicase domain, suggesting that the first CARD domain is accessible for interaction with the MAVS.

Recently, it is reported that RIG-I is constitutively phosphorylated under physiological condition, and this phosphorylation inhibits its antiviral activity (Maharaj et al., 2012). To find out whether phosphorylation of RIG-I directly inhibits its interaction with the downstream adaptor protein MAVS, we tested interactions between the CARD domain of MAVS and the phosphorylation-mimicking mutants of RIG-I S8E and T170E. Our results showed that phosphorylation-mimicking of RIG-I disrupted MAVS binding regardless of dsRNA and ATP (Fig. 5C), indicating that phosphorylation negatively regulated RIG-I-mediated MAVS antiviral signaling not only by inhibiting TRIM25 and polyUb chains binding, but also by directly blocking its interaction with MAVS. We then modeled RIG-I-MAVS signaling transduction through CARD-CARD interaction regulated by phosphorylation (Fig. 5D). In the resting state, residues S8 and T170 of the CARD domains of RIG-I are constitutively phosphorylated, which blocks the RIG-I interaction with the CARD domain of MAVS. Dephosphorylation of the CARD domains of RIG-I enables their binding to MAVS and subsequently initiates antiviral signaling.

DISCUSSION

The electron microscopic structure of RIG-I in complex with blunt-ended dsRNA as a 2:2 molar ratio indicated conformational rearrangements of the tandem CARD domains of RIG-I occur in the presence of dsRNA. RIG-I specifically binds to unanchored K63-linked polyUb and phosphorylation mimicking mutations of RIG-I impairs binding of both unanchored K63-linked polyUb and TRIM25, as well as inhibits RIG-I interaction with MAVS.

Upon viral infection, dsRNA is recognized by the CTD of RIG-I, which induces a conformational change of RIG-I in the presence of ATP and facilitates the recruitment of a series of signaling molecules. The tandem CARD domains of RIG-I affect the CARD domain of MAVS, triggering antiviral responses. RNA transcripts containing a 5′ triphosphate (ppp) represents a major ligand species of RIG-I (Hornung et al., 2006; Pichlmair et al., 2006). Synthetic dsRNA or short dsRNA mimetics derived from RNase digestion of poly I:C are also recognized by the CTD (Kato et al., 2008; Takahasi et al., 2008). Recent studies demonstrated that the CTD of RIG-I can bind blunt-ended dsRNA as well, although with lower affinity when compared with 5′ppp dsRNA (Schlee et al., 2009; Lu et al., 2011). Our results confirmed that blunt ended dsRNA can bind to full length RIG-I and trigger its conformational changes only in the presence of ATP. Moreover, EM analysis of full length RIG-I in complex with blunt-ended dsRNA revealed a stoichiometry of 2:2.

Post-translational modification (PTM) is a mechanism for regulation of various proteins involved in cellular signaling pathways. Ubiquitination and phosphorylation contribute to

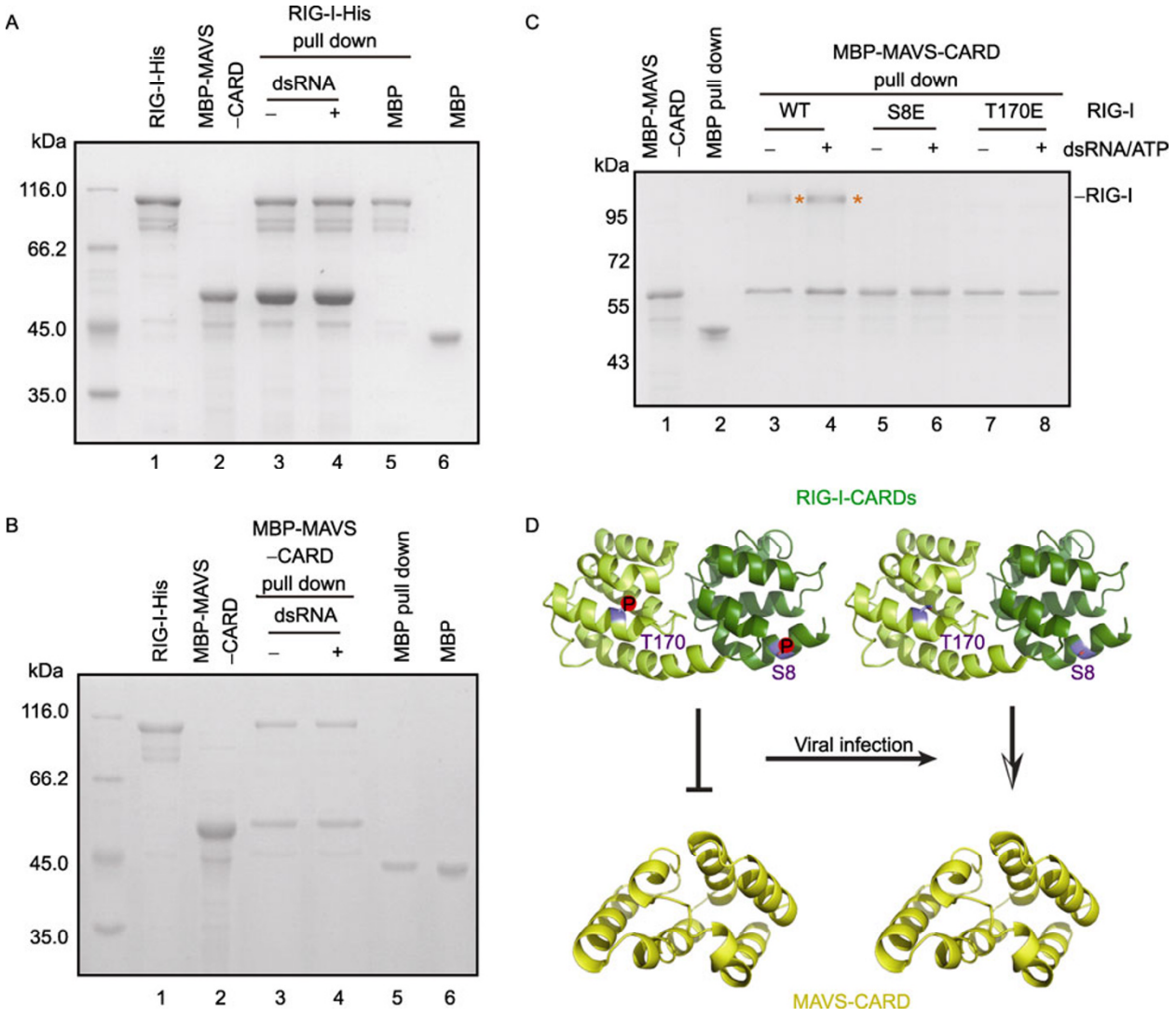

Figure 5. Phosphorylation-mimicking at S8 and T170 inhibits RIG-I interaction with MAVS. (A and B) Wild-type (WT) full length RIG-I binds to MAVS-CARD domain independent of dsRNA. Purified wild-type RIG-I-His and MBP-MAVS-CARD proteins were used in pull-down assays. MBP was used as control. Samples of His pull-down (A) and MBP pull-down (B) were analyzed by SDS-PAGE. (C) RIG-I mutants S8E and T170E showed decreased interaction with the CARD domain of MAVS. MBP-MAVS-CARD proteins were incubated with wild-type or mutant (S8E or T170E) RIG-I with and without dsRNA. The asterisks indicate RIG-I pulled down by MBP-MAVS-CARD. (D) A model of RIG-I CARDs interacting with MAVS-CARD domain. Phosphorylation of RIG-I at S8 and T170 (colored in slate) inhibits the signaling transduction mediated by CARD-CARD interaction. After dephosphorylation of the CARD domains (colored in green), RIG-I is activated to interact with MAVS-CARD domain (colored in yellow).

distinct regulatory activities of signaling pathways (Oh et al., 2007). RIG-I is ubiquitinated at K172 by the E3 ubiquitin ligaseTRIM25 (Gack et al., 2007). T55I mutation of RIG-I decreases the level of TRIM25 binding, leading to reduced ubiquitination of RIG-I and downstream MAVS signaling. In addition, several other ubiquitin ligases including Riplet and RNF125 regulate the activation of RIG-I (Oshiumi et al., 2009, 2010). RNF125 conjugates K48-linked polyUb to RIG-I, leading to proteasomal degradation and down-regulation of IFN species produced (Arimoto et al., 2007). Unanchored K63-linked polyUb activate RIG-I and induce expression of IFN-β (Zeng et al., 2010).

We have found that RIG-I can bind to K63-linked polyUb with suboptimal affinity in the absence of dsRNA, while phosphorylation-mimicking of RIG-I abrogates polyUb binding. Viral dsRNA induced conformational rearrangements of the tandem CARD domains appear essential to facilitate optimal binding of TRIM25 or unanchored K63-linked polyUb, which is required for activation of RIG-I.

The phosphorylation level of RIG-I is reduced upon viral

infection, indicating an activation mechanism by dephosphorylation (Maharaj et al., 2012). Our results showed that phosphorylation-mimicking mutants of RIG-I S8E or T170E dramatically decreased or abolished binding of TRIM25, unanchored K63-linked polyUb, and MAVS, indicating redundant inhibitory effects on RIG-I signaling. Homology modeling of the CARD domains of human RIG-I explains the structural basis of inhibition by phosphorylation. Since T170 and K172 are immediately adjacent to each other, phosphorylation of T170 will alter the surface charge and therefore sterically hinder the binding of unanchored K63-linked polyUb, as well as TRIM25-mediated polyUb attachment to K172. Residue S8 is in close proximity to the C-terminus of the first CARD domain, and may indirectly influence the ubiquitin binding sites around residues K154, K164 and K172 in the second CARD domain (Nistal-Villan et al., 2010). Further structural studies are required to elucidate the atomic details of phosphorylation and polyUb-mediated regulation of RIG-I signaling.

Unanchored polyUb chains appear to induce high-order clustering of RIG-I promoting MAVS-mediated antiviral signaling cascades (Jiang et al., 2012). TRIM25-mediated K63-linked ubiquitination of RIG-I and binding of unanchored K63-linked polyUb may thus play equivalent roles during aggregation of the tandem CARD domains of RIG-I.

We propose a model of regulation of RIG-I-mediated antiviral signaling (Fig. 6). Under physiological conditions, S8 and T170 of RIG-I are constitutively phosphorylated to maintain an autoinhibitory state. During viral infection, dsRNA is recognized by the CTD of RIG-I, which induces dimerization and conformational rearrangements of RIG-I in the presence of ATP, leading to optimal binding of TRIM25 and K63-linked polyUb. Dephosphorylation at sites S8 and T170 removes the steric hindrance and alters the surface charges. As a result, both TRIM25-mediated ubiquitination of RIG-I and binding of unanchored K63-linked polyUb can promote high-order oligomerization of RIG-I (Jiang et al., 2012), which subsequently interacts with the CARD domain of MAVS, leading to aggregates of MAVS (Hou et al., 2011). Activated MAVS then triggers downstream signaling by molecules including IKK, TBK1, NF-κB and IRF3.

MATERIALS AND METHODS

Cloning, protein expression and purification

The cDNA encoding full length human RIG-I (amino acids 1–925) was cloned into expression vector pET28a. Mutations of S8E, T55I, T170E and K172R of RIG-I were generated by QuikChange Site-directed Mutagenesis kit (Stratagene) and verified by sequenc-

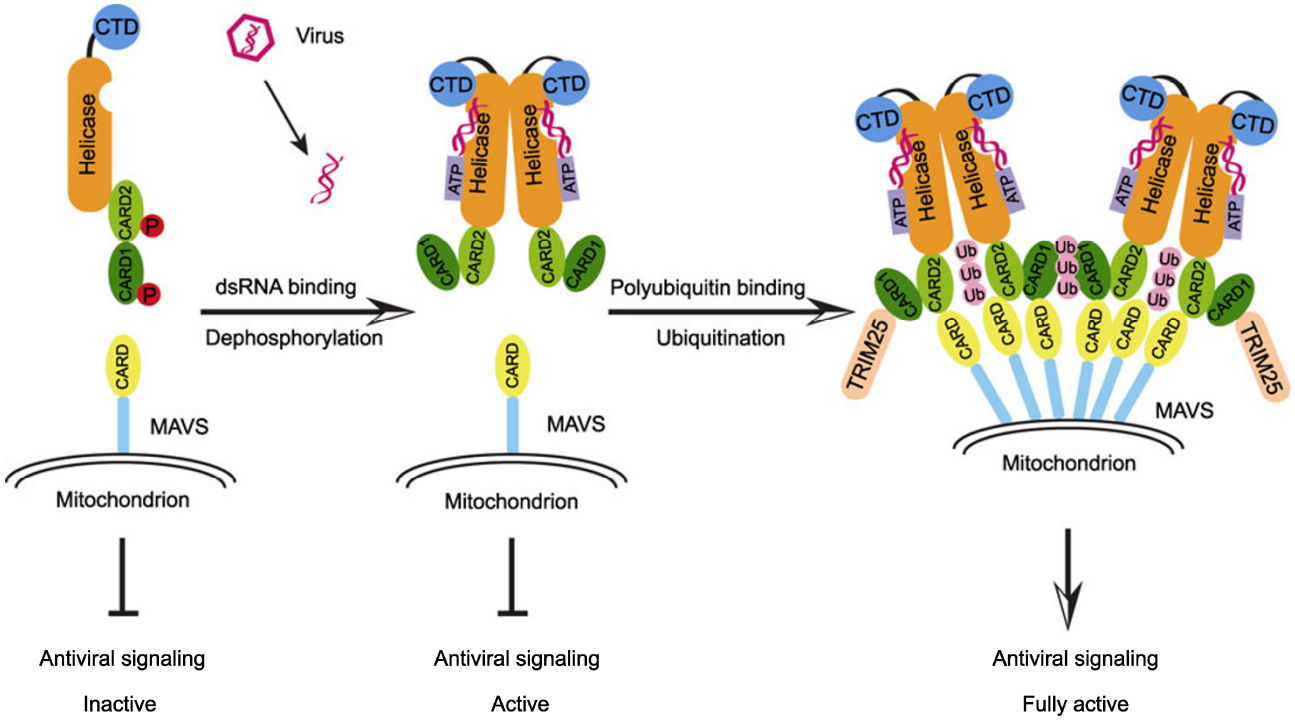

Figure 6. Model of RIG-I-mediated antiviral signaling. (A) Inactive RIG-I is a monomer in autosupressed state. Residues S8 and T170 of the CARD domains are phosphorylated, which impairs the interaction between RIG-I and downstream protein MAVS. (B) Viral infection induces the dimerization and dephosphorylation of RIG-I. Virus-derived dsRNA binds and triggers conformational rearrangements of the tandem CARD domains. RIG-I is activated and ready to recruit additional molecules for signal augmentation. (C) Full activationof RIG-I. TRIM25-mediated ubiquitination and/or binding of unanchored K63-linked polyUb can promote higher-order oligomerization of RIG-I, leading to enhanced CARD-CARD interactions with downstream protein MAVS. As a result, MAVS forms aggregates for efficient antiviral signaling.

ing. All the constructs of RIG-I with a C-terminal 6x His-tag (RIG-I-His) were transformed into *E.coli* BL21 (DE3) codon plus competent cells. Protein expression was induced by adding 0.5 mmol/L isopropyl β-D-thiogalactopyranoside (IPTG) in Terrific Broth medium at 16°C for 18 h. Bacterial cells were harvested and proteins were purified at 4°C on Ni^{2+}-NTA affinity column, followed by gel filtration and ion exchange chromatography. Full length TRIM25 (amino acids 1–630) and MAVS-CARD domain (amino acids 1–93) were cloned into vector MBP-pET-28a, which was modified from pET-28a (Novagen), and expressed in *E.coli* BL21 (DE3) cells. MBP-TRIM25 and MBP-MAVS-CARD fusion proteins were purified by amylase resin column, followed by gel filtration chromatography. All proteins were stored in buffer A containing 20 mmol/L HEPES (pH 7.5), 100 mmol/L NaCl and 1 mmol/L DTT.

RIG-I dimerization analysis by gel filtration

The 14-bp blunt-ended dsRNA (5′-GGCGCGCGCGCGCC-3′) used in this experiment was chemically synthesized as described previously (Lu et al., 2011). Purified RIG-I protein was mixed with dsRNA in different molar ratio at 4°C for 30 min. 250 μL samples (1 mg/mL) were injected into Superdex-200 (10/300 GL) gel filtration column (GE Healthcare) with buffer A. The column was calibrated with standard proteins of different molecular weights.

Isothermal titration calorimetry (ITC)

ITC experiments were carried out at 20°C using a VP-ITC microcalorimeter (MicroCal Inc.). Protein samples were desalted into a buffer containing 20 mmol/L HEPES (pH 7.5), 100 mmol/L NaCl. To analyze the binding of dsRNA with full length RIG-I, dsRNA was injected into the calorimetric cell containing RIG-I at 10 μmol/L in the presence or absence of ATP. Titrations were performed with twenty 2 μL injection, and with 300 sec equilibration time between injections. The ITC data were analyzed using the Origin version 7.0 program and fitted to a single-site binding model to obtain the parameters *K*d, ΔH, and stoichiometry (N).

Dynamic light scattering

The weighted distribution and homogenicity of full length RIG-I mixed with dsRNA in different molar ratios were determined at 25°C by dynamic light scattering. Briefly, RIG-I was diluted to 1.5 mg/ml and mixed with dsRNA at 4°C for 30 min in molar ratio 1:2, 2:1 and 1:1, respectively. Scattered light was measured at a 90° angle using a 658 nm wavelength.

Pull-down assays

MBP-tagged bait proteins were coupled on amylase resin first, and then mixed with different prey proteins at 4°C for 1 h in buffer A. The mixtures were washed three times with the same buffer. The input and output samples were boiled in SDS-PAGE loading buffer and loaded on SDS-PAGE followed by Coomassie blue staining. The procedure of His pull-down assays was similar to MBP pull-down, but the mixtures were washed with buffer A with 50 mmol/L imidazole.

Western blot

Samples of pull down assays were boiled and separated electrophorectically on 12% SDS-PAGE gel. Protein bands were transferred onto PVDF (polyvinylidene fluoride) membrane by electroblotting. The membrane was blocked in TBST buffer (25 mmol/L Tris-HCl pH 7.4, 1.5 mol/L NaCl, 0.5% Tween-20) containing 5% fat-free dry milk for 1 h. The membrane was washed with TBST for three times and incubated with mouse anti-Ub and anti-His antibody for 2 h, respectively. After washing with TBST, the membrane sheets were incubated with peroxidase conjugated anti-mouse antibody for 1 h. The bands were visualized using Thermo ECL detection kit.

EM data collection

RIG-I dimer with RNA sample was analyzed by negative-stain electron microscopy. The sample was first diluted to 6.7 μg/ml, then 4–5 μL of such sample was deposited onto a glow-discharged 400/200 mesh carbon grid (1.2 × 1.3 μm hole size) before stained with 2% uranyl acetate. Data were collected by utilizing a Tecnai TF20 transmission electron microscope (FEI Company, USA) operated at an acceleration voltage of 200 kV. Micrograph images were acquired at a nominal microscopic magnification of 100,000 using a 4k × 4k CCD camera. Images were collected at a defocus ranging from –0.3 to –0.6 μm with a pixel size of 1.1 Å/pixel.

EM image processing and model building

10,991 particles were boxed out from 176 CCD images by *e2boxer.py* program of EMAN2 (Tang et al., 2007). Reference-free class-averages were generated by *e2refine2d.py* program, and those class-averages were used to calculate an initial model by *e2initialmodel.py* program from EMAN2. Contrast transfer function parameters were estimated using EMAN1 procedure "*ctfit*" (Ludtke et al., 2001). 3D reconstruction by *refine* from EMAN1 (Cong et al., 2010; Cong and Ludtke, 2010) was processed without imposing any symmetry initially, and a 2-fold symmetry was revealed in this reconstruction, which was subsequently imposed in the reconstruction process. The final 3D density map was yielded from about 9,100 particles.

UCSF Chimera *volume measurement* module was used to measure the volume of the map. Situs program *colores*, a full exhaustive search in 6D search space (Wriggers et al., 1999; Chacon and Wriggers, 2002; Wriggers, 2012), was used for rigid-body fitting of the homologous atomic models independently into the density map. The models include the crystal structure of human RIG-I (ΔCARD) in complex with double-stranded RNA (dsRNA) (PDB ID: 3TMI) and a comparative model of CARD domains built from the amino acids sequences of human CARD domains and the crystal structures of duck CARD domains (PDB ID: 4A2W) by the SWISS-MODEL. To get the maximum cross-correlation score between the map and the models, a local refinement program *collage* from Situs was processed to further refine the original multi-fragment model.

ACKNOWLEDGEMENTS

We thank the staff from the Center for Integrative Imaging at Hefei National Laboratory for Physical Sciences at the Microscale for EM data collection, and Dr. Peng Zhang from the Institute of Plant Physiology & Ecology for help of DLS analysis. This work was supported by the National Basic Research Program (973 Program) (Nos.

2010CB529701 and 2012CB910204), the National Natural Science Foundation of China (Grant Nos. 10979005 and 30970566), and the Science and Technology Commission of Shanghai Municipality (11JC14140000). Drs. YC and ZZ are scholars of the Hundred Talents Program of the Chinese Academy of Sciences.

ABBREVIATIONS

CARD, caspase activation and recruitment domain; CLR, C-type lectin receptor; CTD, C-terminal regulatory domain; DLS, dynamic light scattering; dsRNA, double-stranded RNA; EM, electron microscope; ITC, isothermal titration calorimetry; LGP2, laboratory of genetics and physiology 2; MDA5, melanoma differentiation-associated gene 5; NLR, NOD-like receptor; PAMP, pathogen-associated molecular pattern; PKC, Protein kinase C; PRR, pattern recognition receptor; PTM, post-translational modification; RIG-I, Retinoic acid-inducible gene I; RD, repressor domain; TLR, Toll-like receptor

REFERENCES

Arimoto, K., Takahashi, H., Hishiki, T., Konishi, H., Fujita, T., and Shimotohno, K. (2007). Negative regulation of the RIG-I signaling by the ubiquitin ligase RNF125. Proc Natl Acad Sci U S A 104, 7500–7505.

Chacon, P., and Wriggers, W. (2002). Multi-resolution contour-based fitting of macromolecular structures. J Mol Biol 317, 375–384.

Cong, Y., Baker, M.L., Jakana, J., Woolford, D., Miller, E.J., Reissmann, S., Kumar, R.N., Redding-Johanson, A.M., Batth, T.S., and Mukhopadhyay, A. (2010). 4.0-Å resolution cryo-EM structure of the mammalian chaperonin TRiC/CCT reveals its unique subunit arrangement. Proc Natl Acad Sci U S A 107, 4967–4972.

Cong, Y., and Ludtke, S.J. (2010). Single particle analysis at high resolution. Methods Enzymol 482, 211–235.

Gack, M.U., Kirchhofer, A., Shin, Y.C., Inn, K.S., Liang, C., Cui, S., Myong, S., Ha, T., Hopfner, K.P., and Jung, J.U. (2008). Roles of RIG-I N-terminal tandem CARD and splice variant in TRIM25-mediated antiviral signal transduction. Proc Natl Acad Sci U S A 105, 16743–16748.

Gack, M.U., Nistal-Villan, E., Inn, K.S., Garcia-Sastre, A., and Jung, J.U. (2010). Phosphorylation-mediated negative regulation of RIG-I antiviral activity. J Virol 84, 3220–3229.

Gack, M.U., Shin, Y.C., Joo, C.H., Urano, T., Liang, C., Sun, L., Takeuchi, O., Akira, S., Chen, Z., and Inoue, S. (2007). TRIM25 RING-finger E3 ubiquitin ligase is essential for RIG-I-mediated antiviral activity. Nature 446, 916–920.

Hornung, V., Ellegast, J., Kim, S., Brzozka, K., Jung, A., Kato, H., Poeck, H., Akira, S., Conzelmann, K.K., Schlee, M., et al. (2006). 5′-Triphosphate RNA is the ligand for RIG-I. Science 314, 994–997.

Hou, F., Sun, L., Zheng, H., Skaug, B., Jiang, Q.X., and Chen, Z.J. (2011). MAVS forms functional prion-like aggregates to activate and propagate antiviral innate immune response. Cell 146, 448–461.

Janeway, C.A., Jr., and Medzhitov, R. (2002). Innate immune recognition. Annu Rev Immunol 20, 197–216.

Jiang, F., Ramanathan, A., Miller, M.T., Tang, G.Q., Gale, M., Jr., Patel, S.S., and M Ramanathan arcotrigiano, J. (2011). Structural basis of RNA recognition and activation by innate immune receptor RIG-I. Nature 479, 423–427.

Jiang, X., Kinch, L.N., Brautigam, C.A., Chen, X., Du, F., Grishin, N.V., and Chen, Z.J. (2012). Ubiquitin-Induced Oligomerization of the RNA Sensors RIG-I and MDA5 Activates Antiviral Innate Immune Response. Immunity 36, 959–973.

Kato, H., Takeuchi, O., Mikamo-Satoh, E., Hirai, R., Kawai, T., Matsushita, K., Hiiragi, A., Dermody, T.S., Fujita, T., and Akira, S. (2008). Length-dependent recognition of double-stranded ribonucleic acids by retinoic acid-inducible gene-I and melanoma differentiation-associated gene 5. J Exp Med 205, 1601–1610.

Kawai, T., Takahashi, K., Sato, S., Coban, C., Kumar, H., Kato, H., Ishii, K.J., Takeuchi, O., and Akira, S. (2005). IPS-1, an adaptor triggering RIG-I- and Mda5-mediated type I interferon induction. Nat Immunol 6, 981–988.

Kowalinski, E., Lunardi, T., McCarthy, A.A., Louber, J., Brunel, J., Grigorov, B., Gerlier, D., and Cusack, S. (2011). Structural basis for the activation of innate immune pattern-recognition receptor RIG-I by viral RNA. Cell 147, 423–435.

Kumar, H., Kawai, T., and Akira, S. (2009). Pathogen recognition in the innate immune response. Biochem J 420, 1–16.

Leung, D.W., and Amarasinghe, G.K. (2012). Structural insights into RNA recognition and activation of RIG-I-like receptors. Curr Opin Struct Biol 22, 297–303

Liu, H.M., Loo, Y.M., Horner, S.M., Zornetzer, G.A., Katze, M.G., and Gale, M., Jr. (2012). The mitochondrial targeting chaperone 14-3-3epsilon regulates a RIG-I translocon that mediates membrane association and innate antiviral immunity. Cell Host Microbe 11, 528–537.

Lu, C., Ranjith-Kumar, C.T., Hao, L., Kao, C.C., and Li, P. (2011). Crystal structure of RIG-I C-terminal domain bound to blunt-ended double-strand RNA without 5′ triphosphate. Nucleic Acids Res 39, 1565–1575.

Lu, C., Xu, H., Ranjith-Kumar, C.T., Brooks, M.T., Hou, T.Y., Hu, F., Herr, A.B., Strong, R.K., Kao, C.C., and Li, P. (2010). The structural basis of 5′ triphosphate double-stranded RNA recognition by RIG-I C-terminal domain. Structure 18, 1032–1043.

Ludtke, S.J., Baldwin, P.R., and Chiu, W. (1999). EMAN: semiautomated software for high-resolution single-particle reconstructions. J Struct Biol 128, 82–97.

Ludtke, S.J., Jakana, J., Song, J.L., Chuang, D.T., and Chiu, W. (2001). A 11.5 A single particle reconstruction of GroEL using EMAN. J Mol Biol 314, 253–262.

Luo, D., Kohlway, A., Vela, A., and Pyle, A.M. (2012). Visualizing the Determinants of Viral RNA Recognition by Innate Immune Sensor RIG-I. Structure 20, 1983–1988.

Maharaj, N.P., Wies, E., Stoll, A., and Gack, M.U. (2012). Conventional protein kinase C-alpha (PKC-alpha) and PKC-beta negatively regulate RIG-I antiviral signal transduction. J Virol 86, 1358–1371.

Meylan, E., Curran, J., Hofmann, K., Moradpour, D., Binder, M., Bartenschlager, R., and Tschopp, J. (2005). Cardif is an adaptor protein in the RIG-I antiviral pathway and is targeted by hepatitis C virus. Nature 437, 1167–1172.

Nistal-Villan, E., Gack, M.U., Martinez-Delgado, G., Maharaj, N.P., Inn, K.S., Yang, H., Wang, R., Aggarwal, A.K., Jung, J.U., and Garcia-Sastre, A. (2010). Negative role of RIG-I serine 8 phosphorylation in the regulation of interferon-beta production. J

Biol Chem 285, 20252–20261.
Oh, S.D., Lao, J.P., Hwang, P.Y., Taylor, A.F., Smith, G.R., and Hunter, N. (2007). BLM ortholog, Sgs1, prevents aberrant crossing-over by suppressing formation of multichromatid joint molecules. Cell 130, 259–272.
Oshiumi, H., Matsumoto, M., Hatakeyama, S., and Seya, T. (2009). Riplet/RNF135, a RING finger protein, ubiquitinates RIG-I to promote interferon-beta induction during the early phase of viral infection. J Biol Chem 284, 807–817.
Oshiumi, H., Miyashita, M., Inoue, N., Okabe, M., Matsumoto, M., and Seya, T. (2010). The ubiquitin ligase Riplet is essential for RIG-I-dependent innate immune responses to RNA virus infection. Cell Host Microbe 8, 496–509.
Pichlmair, A., Schulz, O., Tan, C.P., Naslund, T.I., Liljestrom, P., Weber, F., and Reis e Sousa, C. (2006). RIG-I-mediated antiviral responses to single-stranded RNA bearing 5′-phosphates. Science 314, 997–1001.
Saito, T., Hirai, R., Loo, Y.M., Owen, D., Johnson, C.L., Sinha, S.C., Akira, S., Fujita, T., and Gale Jr, M. (2007). Regulation of innate antiviral defenses through a shared repressor domain in RIG-I and LGP2. Science's STKE 104, 582.
Schlee, M., Roth, A., Hornung, V., Hagmann, C.A., Wimmenauer, V., Barchet, W., Coch, C., Janke, M., Mihailovic, A., Wardle, G., et al. (2009). Recognition of 5′ triphosphate by RIG-I helicase requires short blunt double-stranded RNA as contained in panhandle of negative-strand virus. Immunity 31, 25–34.
Takahasi, K., Yoneyama, M., Nishihori, T., Hirai, R., Kumeta, H., Narita, R., Gale, M., Jr., Inagaki, F., and Fujita, T. (2008). Nonself RNA-sensing mechanism of RIG-I helicase and activation of antiviral immune responses. Mol Cell 29, 428–440.
Takeuchi, O., and Akira, S. (2010). Pattern recognition receptors and inflammation. Cell 140, 805–820.
Tang, G., Peng, L., Baldwin, P.R., Mann, D.S., Jiang, W., Rees, I., and Ludtke, S.J. (2007). EMAN2: an extensible image processing suite for electron microscopy. J Struct Biol 157, 38–46.
Wriggers, W. (2012). Conventions and workflows for using Situs. Acta Crystallogr D Biol Crystallogr 68, 344–351.
Wriggers, W., Milligan, R.A., and McCammon, J.A. (1999). Situs: A package for docking crystal structures into low-resolution maps from electron microscopy. J Struct Biol 125, 185–195.
Xu, L.G., Wang, Y.Y., Han, K.J., Li, L.Y., Zhai, Z., and Shu, H.B. (2005). VISA is an adapter protein required for virus-triggered IFN-beta signaling. Mol Cell 19, 727–740.
Yoneyama, M., Kikuchi, M., Matsumoto, K., Imaizumi, T., Miyagishi, M., Taira, K., Foy, E., Loo, Y.M., Gale, M., Jr., Akira, S., et al. (2005). Shared and unique functions of the DExD/H-box helicases RIG-I, MDA5, and LGP2 in antiviral innate immunity. J Immunol 175, 2851–2858.
Yoneyama, M., Kikuchi, M., Natsukawa, T., Shinobu, N., Imaizumi, T., Miyagishi, M., Taira, K., Akira, S., and Fujita, T. (2004). The RNA helicase RIG-I has an essential function in double-stranded RNA-induced innate antiviral responses. Nat Immunol 5, 730–737.
Zeng, W., Sun, L., Jiang, X., Chen, X., Hou, F., Adhikari, A., Xu, M., and Chen, Z.J. (2010). Reconstitution of the RIG-I pathway reveals a signaling role of unanchored polyubiquitin chains in innate immunity. Cell 141, 315–330.